Research Article

Chih-Jen Yu*, Chih-Ching Ho and I-Hsuan Chen

Heterodyne interferometric fiber-optic gyroscope

https://doi.org/10.1515/phys-2025-0229
Received April 30, 2025; accepted October 6, 2025;
published online December 9, 2025

Abstract: This study proposes the theoretical design of an optical setup of a heterodyne interferometric fiber-optic gyroscope (HIFOG). The polarized IFOG utilizes a coherent light source and an electro-optic modulator to generate a dual-frequency laser light source. The Sagnac interferometric signal can be measured from the amplitude term of the temporal interference fringe as well as beat frequency signal. The beat frequency signal can be processed using filtering techniques or the lock-in technique to enhance the signal-to-noise ratio. This approach effectively reduces external environmental noise interference in the interferometric fiber-optic gyroscope, as well as the polarization state changes caused by fiber birefringence.

Keywords: interferometric fiber-optic gyroscope; Sagnac effect; single mode fiber; birefringence

Abbreviations

AC	alternative current
CCW	counterclockwise
CW	clockwise
DC	direct current
DIFOG	depolarized interferometric fiber-optic gyroscope
EOM	electro-optic modulator
FOG	fiber-optic gyroscope
HIFOG	heterodyne interferometric fiber-optic gyroscope
IFOG	interferometric fiber-optic gyroscope
LPR	linear polarization rotator
MEMS	micro-electromechanical systems
NPBS	non-polarizing beam splitter
PIFOG	polarizing interferometric fiber-optic gyroscope
PMD	polarization mode dispersion
SMF	single-mode fiber
SNR	signal-to-noise ratio

***Corresponding author: Chih-Jen Yu**, Graduate Institute of Electro-Optical Engineering, Chang Gung University, NO. 259, Wen-Hwa 1st Road, Guishan District, Taoyuan City 333, Taiwan, ROC,
E-mail: cjyu@mail.cgu.edu.tw
Chih-Ching Ho and I-Hsuan Chen, Graduate Institute of Electro-Optical Engineering, Chang Gung University, NO. 259, Wen-Hwa 1st Road, Guishan District, Taoyuan City 333, Taiwan, ROC

1 Introduction

A gyroscope is a sensing device used to measure the rotational rate of an object and is an essential component in aerospace applications. Currently, rotational rate measurements can be performed using traditional mechanical gyroscopes, micro-electromechanical systems (MEMS) gyroscopes [1, 2], ring laser gyroscopes [3–5], and interferometric fiber-optic gyroscopes (IFOGs) [6], where the sensitivity of an IFOG can be enhanced by increasing the number of fiber coil turns [7].

Conventional IFOGs face a significant challenge posed by fiber birefringence, arising particularly from the bending-induced stress of the coiled fiber. This effect results in zero-bias error and degrades the signal through polarization-related mechanisms [8, 9]. To mitigate these effects, depolarized IFOGs (DIFOGs) are commonly implemented, wherein a depolarizer converts polarized light into unpolarized light, thereby reducing polarization noise at the cost of reduced interference visibility [7, 9, 10].

In recent years, the polarizing interferometric fiber-optic gyroscope (PIFOG) has evolved significantly, with growing interest in architectures employing single-mode fiber (SMF) and laser light sources due to their potential for high-performance navigation and attitude control. By leveraging high-coherence laser sources, this alternative approach suppresses backscattering-induced phase noise while improving scale factor stability, thereby addressing a critical requirement for high-precision aerospace and defense applications [11, 12]. Compared to conventional broadband sources, lasers offer narrow linewidth and exceptional wavelength stability, enabling scale factor accuracies better than 1 part per million [11]. Furthermore, the low attenuation (0.2 dB/km) [13] and inherently low backscattering of SMF make it particularly suitable for laser-driven systems, contributing to significantly improved signal-to-noise ratios (SNRs). In contrast, air-core photonic bandgap fibers, despite their reduced Kerr effect, exhibit high attenuation (∼13 dB/km) [14] and are prone

to higher-order mode coupling, which can degrade overall performance.

Emerging IFOG architectures have begun to leverage fully polarized laser sources together with polarizing components to actively suppress birefringence-induced phase errors, thereby improving signal quality and system sensitivity without the need for depolarizers. Building on this trend, this study introduces a heterodyne interferometry approach based on a dual-frequency laser source combined with tailored polarization control elements. This method effectively mitigates the birefringent effects inherent in standard SMF, which are a major source of phase error in conventional designs.

A key distinction of our approach from traditional heterodyne FOGs [15–17] is the deliberate use of low-cost SMF as the sensing coil. Whereas conventional heterodyne FOGs often rely on polarization-maintaining fiber (PMF) to passively avoid birefringence effects, our system actively compensates for these effects through optical and signal processing means. This shift offers a significant potential reduction in the cost and complexity of the sensing coil, which is a critical component in practical deployments. Furthermore, the Sagnac phase shift is precisely extracted from a time-domain beat signal, a process enhanced by lock-in amplification technique for superior SNR. This combination of active birefringence compensation in standard fiber and advanced electronic detection provides a robust and cost-effective pathway toward high-stability, high-precision fiber-optic gyroscopes for tactical and inertial-grade applications.

2 Basic theory

2.1 Polarization effect of the fiber coil

Consider a fiber coil subjected to fiber bending, temperature effect and mechanical stress induced birefringence, which alters the polarization state of the incident light wave. This effect is referred to as the polarization effect of the fiber coil, and its polarization transfer function can be represented using the Jones matrix as [8]:

$$\begin{aligned}\mathbf{S_{21}} &= \exp(i\overline{\varphi})\begin{pmatrix} a & -b \\ b^* & a^* \end{pmatrix} \\ &= \exp(i\overline{\varphi})\begin{pmatrix} \cos\theta\,\exp\left(i\frac{\xi}{2}\right) & -\sin\theta\,\exp\left(i\frac{\varphi}{2}\right) \\ \sin\theta\,\exp\left(-i\frac{\varphi}{2}\right) & \cos\theta\,\exp\left(-i\frac{\xi}{2}\right) \end{pmatrix},\end{aligned} \tag{1}$$

and

$$\begin{aligned}\mathbf{S_{12}} &= \exp(i\overline{\varphi})\begin{pmatrix} a & b^* \\ -b & a^* \end{pmatrix} \\ &= \exp(i\overline{\varphi})\begin{pmatrix} \cos\theta\,\exp\left(i\frac{\xi}{2}\right) & \sin\theta\,\exp\left(-i\frac{\varphi}{2}\right) \\ -\sin\theta\,\exp\left(i\frac{\varphi}{2}\right) & \cos\theta\,\exp\left(-i\frac{\xi}{2}\right) \end{pmatrix}.\end{aligned} \tag{2}$$

where the subscript 12 and 21 respectively stand for the clockwise (CW, from end 2 to end 1) and counterclockwise (CCW, from end 2 to end 1) propagation directions, $\overline{\varphi}$ is the average phase shift along the fiber, a and b are complex function, ξ is the change of the ellipticity, θ is the rotation angle, and φ is the reciprocal phase of the SMF coil. The birefringent parameters, ξ, θ, and φ are as a function of the fiber length L.

2.2 Dual-frequency laser light source

The central innovation of this study is its light source, namely a dual-frequency laser [18]. The unique characteristics of this light source allow the interferometric signal of the Sagnac loop interferometer to be carried within time-domain interference fringes, which helps improve the SNR.

The dual-frequency laser generates two orthogonal linearly polarized components with a slight frequency difference. A Zeeman He–Ne laser inherently exhibits these characteristics [19].

An alternative method, as shown in Figure 1, utilizes a single-wavelength laser and an electro-optic modulator (EOM) driven by a high-voltage sawtooth signal [18]. The polarization state is then described by the Jones vector:

$$\mathbf{E_{DL}} = \frac{1}{\sqrt{2}}\begin{pmatrix} \exp\left(i\frac{\omega t}{2}\right) \\ \exp\left(-i\frac{\omega t}{2}\right) \end{pmatrix} A\,\exp(i\omega_0 t) \tag{3}$$

Here, A represents the amplitude of the dual-frequency laser source, ω_0 is the central frequency of the single-wavelength laser source, and ω is the driving signal frequency of the EOM, typically ranging from kHz to MHz. From Eq. (3), it can be observed that the frequency of the x-component of the laser beam's electric field is $\omega_0 + (\omega/2)$, while the frequency of the y-component is $\omega_0 - (\omega/2)$. The frequency difference between these two orthogonal electric field components equals the driving frequency of the EOM.

When this dual-frequency laser passes through a quarter-wave plate, it becomes a linearly polarized modulated light source, also known as a linear polarization rotator (LPR) [20, 21],

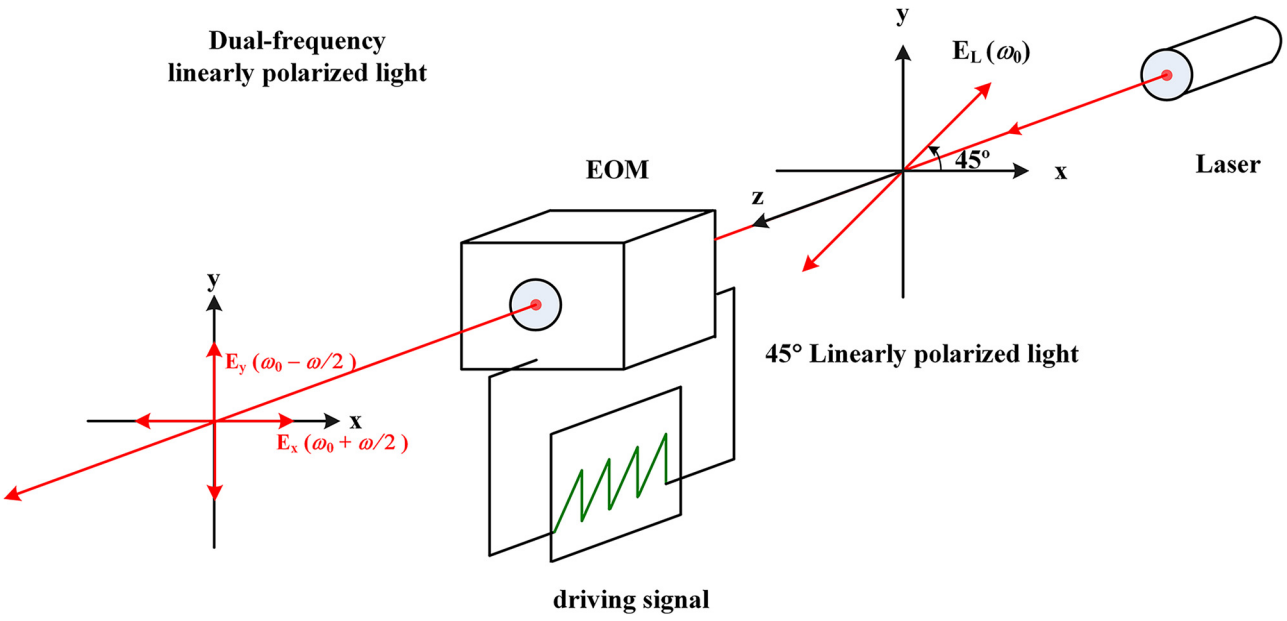

Figure 1: Optical setup of a dual-frequency laser composed by a single frequency laser and an electro-optic modulator. EOM: electro-optic modulator.

$$\mathbf{E}_{\mathbf{LPR}}(\omega) = \begin{pmatrix} \sin\left(\frac{\omega t}{2} + \frac{\pi}{4}\right) \\ \cos\left(\frac{\omega t}{2} + \frac{\pi}{4}\right) \end{pmatrix}. \quad (4)$$

Equation (4) represents the normalized Jones vector of the linearly polarized modulated light source with an intensity value of 1.

3 Optical setup

Figure 2 shows the optical setup of a heterodyne interferometric fiber-optic gyroscope (HIFOG). The incident light used here is the previously mentioned LPR light source. The incident beam is split by the first non-polarizing beam splitter ($NPBS_1$). The transmitted and reflected beams are designated as the signal beam and reference beam, respectively. The signal beam is first transmitted through a polarizer with a horizontal transmission axis and is subsequently split by $NPBS_2$ into two components: the transmitted signal beam and the reflected signal beam. These designations will be used to describe the optical paths and electric fields in the following analysis.

The transmitted signal beam travels CCW through an EOM, the Sagnac loop formed by the fiber coil, then passes again through the transmission side of the $NPBS_2$, and finally goes through an analyzer with its transmission axis set horizontally.

The reflected signal beam, on the other hand, travels CW through the Sagnac loop, an EOM then passes again through the reflection side of the $NPBS_2$, and finally goes through an analyzer with its transmission axis set horizontally.

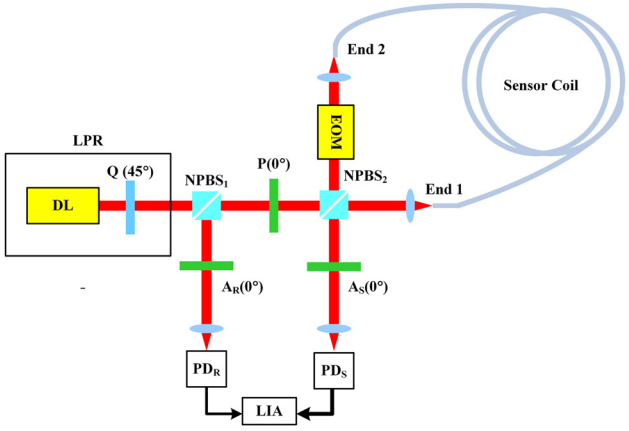

Figure 2: Optical setup of a heterodyne interferometric fiber-optic gyroscope (HIFOG). DL: dual-frequency laser, Q: quarter wave plate, LPR: linear polarization rotator, $NPBS_1$ and $NPBS_2$: non-polarizing beam splitters, P: polarizer, A_R and A_S: analyzer, PD_R and PD_S: photodetectors, LIA: lock-in amplifier.

The electric fields of the transmitted and reflected signal beams are derived using Jones calculus as:

$$\begin{aligned} \mathbf{E}_{\mathbf{ccw}} &= \mathbf{A}(0^\circ)\mathbf{T}_{\mathbf{BS}}\mathbf{S}_{21}\mathbf{T}_{\mathbf{BS2}}\mathbf{P}(0^\circ)\mathbf{T}_{\mathbf{BS1}}\mathbf{E}_{\mathbf{LPR}}(\omega) \\ &= \exp\left(i\varphi_{\mathrm{ccw}} - \frac{\varphi_m}{2}\right)\begin{pmatrix} 1 & 0 \\ 0 & 0 \end{pmatrix}\frac{1}{\sqrt{2}}\begin{pmatrix} 1 & 0 \\ 0 & 1 \end{pmatrix} \\ &\times \begin{pmatrix} a & -b \\ b^* & a^* \end{pmatrix}\frac{1}{\sqrt{2}}\begin{pmatrix} 1 & 0 \\ 0 & 1 \end{pmatrix}\begin{pmatrix} 1 & 0 \\ 0 & 0 \end{pmatrix} \end{aligned}$$

$$\times \frac{1}{\sqrt{2}}\begin{pmatrix}1 & 0\\ 0 & 1\end{pmatrix}\begin{pmatrix}\sin\left(\frac{\omega t}{2}+\frac{\pi}{4}\right)\\ \cos\left(\frac{\omega t}{2}+\frac{\pi}{4}\right)\end{pmatrix}$$

$$= \frac{1}{2\sqrt{2}} a \sin\left(\frac{\omega t}{2}+\frac{\pi}{4}\right)\exp\left(i\varphi_{\mathrm{ccw}}-\frac{\varphi_m}{2}\right)\begin{pmatrix}1\\ 0\end{pmatrix}, \quad (5)$$

and

$$\begin{aligned}\mathbf{E_{cw}} &= \mathbf{A}(0^\circ)\mathbf{R_{BS}}\mathbf{S_{12}}\mathbf{R_{BS2}}\mathbf{P}(0^\circ)\mathbf{T_{BS1}}\mathbf{E_{LRP}}(\omega)\\ &= \exp\left(i\varphi_{\mathrm{cw}}+\frac{\varphi_m}{2}\right)\begin{pmatrix}1 & 0\\ 0 & 0\end{pmatrix}\frac{1}{\sqrt{2}}\begin{pmatrix}1 & 0\\ 0 & 1\end{pmatrix}\\ &\times\begin{pmatrix}a & b^*\\ -b & a^*\end{pmatrix}\frac{1}{\sqrt{2}}\begin{pmatrix}1 & 0\\ 0 & 1\end{pmatrix}\begin{pmatrix}1 & 0\\ 0 & 0\end{pmatrix}\\ &\times\frac{1}{\sqrt{2}}\begin{pmatrix}1 & 0\\ 0 & 1\end{pmatrix}\begin{pmatrix}\sin\left(\frac{\omega t}{2}+\frac{\pi}{4}\right)\\ \cos\left(\frac{\omega t}{2}+\frac{\pi}{4}\right)\end{pmatrix}\\ &= \frac{1}{2\sqrt{2}} a \sin\left(\frac{\omega t}{2}+\frac{\pi}{4}\right)\exp\left(i\varphi_{\mathrm{cw}}+\frac{\varphi_m}{2}\right)\begin{pmatrix}1\\ 0\end{pmatrix}.\end{aligned} \quad (6)$$

As described by Eqs. (5) and (6), the fundamental phase shifts φ_{cw} and φ_{ccw} are due to the unidirectional propagation of light within the rotating Sagnac loop. The additional phase components of $\pm\varphi_m/2$ are imparted by the EOM's bias phase in conjunction with the temporal delay of the fiber coil [22]. These additional phase components are the crucial parameters employed to enhance the sensitivity, as will be explained later.

$$\mathbf{P}(0^\circ) = \mathbf{A}(0^\circ) = \begin{pmatrix}1 & 0\\ 0 & 0\end{pmatrix}, \quad (7)$$

represent the Jones matrices of a polarizer and an analyzer with their transmission axes set at 0°, respectively.

$$\mathbf{T_{BS}} = \mathbf{R_{BS}} = \frac{1}{\sqrt{2}}\begin{pmatrix}1 & 0\\ 0 & 1\end{pmatrix}, \quad (8)$$

represent the Jones matrices of the transmission and reflection surfaces of the NPBS, respectively. The two superimposed electric fields of the CW, and CCW propagating light waves, $\mathbf{E_{cw}}$ and $\mathbf{E_{ccw}}$, after passing through the analyzers, form the output electric field of the optical system. The output electric field, $\mathbf{E_{sig}}$, can be expressed as a Jones vector:

$$\begin{aligned}\mathbf{E_{sig}} &= \mathbf{E_{cw}} + \mathbf{E_{ccw}} = \frac{1}{2\sqrt{2}} a \sin\left(\frac{\omega t}{2}+\frac{\pi}{4}\right)\begin{pmatrix}1\\ 0\end{pmatrix}\\ &\times\left[\exp\left(i\varphi_{\mathrm{cw}}+\frac{\varphi_m}{2}\right)+\exp\left(i\varphi_{\mathrm{ccw}}-\frac{\varphi_m}{2}\right)\right].\end{aligned} \quad (9)$$

The optical intensity signal received by the photodetector $\mathrm{PD_S}$ after the output light passes through it can be expressed as:

$$\begin{aligned}I_{\mathrm{sig}} &= \mathbf{E}^*_{\mathbf{sig}}\cdot\mathbf{E_{sig}} = \frac{1}{8}\cos^2\theta\left[2+2\cos\left(\varphi_{\mathrm{cw}}-\varphi_{\mathrm{ccw}}+\varphi_m\right)\right]\\ &\times\frac{1}{2}\left[1-\cos\left(\omega t+\frac{\pi}{2}\right)\right]\\ &= \frac{1}{8}\cos^2\theta\left[1+\cos\left(\varphi_{\mathrm{sag}}+\varphi_m\right)\right](1+\sin\omega t)\\ &= \bar{I}_{\mathrm{sig}}+\tilde{I}_{\mathrm{sig}}\sin\omega t.\end{aligned} \quad (10)$$

The Sagnac phase, φ_{sag}, is the phase difference between the CW and CCW beams,

$$\varphi_{\mathrm{sag}} = \varphi_{\mathrm{cw}} - \varphi_{\mathrm{ccw}} = \frac{8N\pi^2R^2\Omega}{\lambda c}, \quad (11)$$

where N and R are the coil number and radius of the fiber coil, respectively, Ω is the angular velocity, λ is the wavelength, and c is the wave velocity in vacuum. From Eq. (10), it can be observed that the light intensity signal exhibits reciprocity. The coherence length of standard frequency-stabilized lasers can extend to approximately 100 m, significantly exceeding the optical path difference produced in a Sagnac interferometer. As indicated in Eq. (10), the high coherence of the laser source enables the generation of a beat signal with ideal interference visibility. Figure 3 schematically illustrates the optical intensity signal measured at the photodetector as a function of the Sagnac phase shift. This signal can be extracted from either the DC component or the AC (beat-frequency) component in Eq. (10), both of which exhibit the same interference pattern as depicted. However, due to the higher susceptibility of the DC signal to noise, this study emphasizes AC signal detection. To further improve the SNR, a lock-in amplification technique is employed [23], which utilizes correlation processing between the detected signal and a reference signal. For a detailed description of the lock-in amplification method, please refer to reference [24].

As described earlier, the reference signal in Figure 2 is generated by splitting a portion of the incident laser beam at $\mathrm{NPBS_1}$ and is detected by the photodetector $\mathrm{PD_R}$. The corresponding electric field can be expressed as:

$$\begin{aligned}\mathbf{E_{ref}} &= \mathbf{A}(0^\circ)\mathbf{R_{BS1}}\mathbf{E_{LPR}}(\omega)\\ &= \begin{pmatrix}1 & 0\\ 0 & 0\end{pmatrix}\frac{1}{\sqrt{2}}\begin{pmatrix}1 & 0\\ 0 & 1\end{pmatrix}\begin{pmatrix}\sin\left(\frac{\omega t}{2}+\frac{\pi}{4}\right)\\ \cos\left(\frac{\omega t}{2}+\frac{\pi}{4}\right)\end{pmatrix}\\ &= \frac{1}{\sqrt{2}}\sin\left(\frac{\omega t}{2}+\frac{\pi}{4}\right)\begin{pmatrix}1\\ 0\end{pmatrix}.\end{aligned} \quad (12)$$

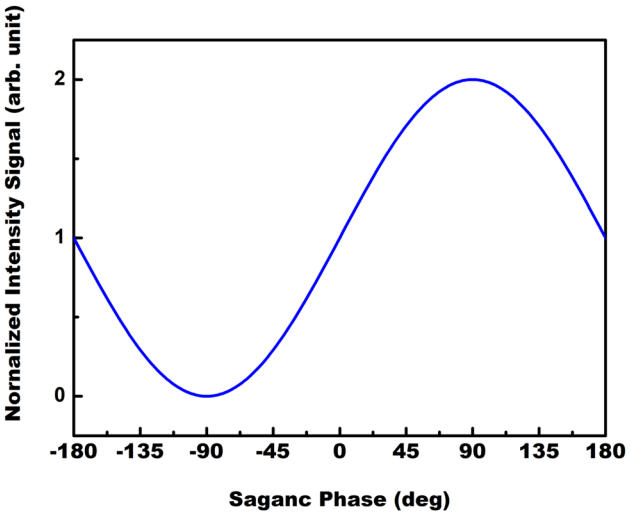

Figure 3: Normalized intensity versus Sagnac phase, showing the enhanced sensitivity achieved by operating the interferometer with a phase bias near zero phase shift.

Thus, the intensity of this reference signal can be expressed as:

$$I_{\text{ref}} = \mathbf{E}^{*}_{\mathbf{ref}} \cdot \mathbf{E}_{\mathbf{ref}} = \frac{1}{4}\left(1 + \sin\,\omega t\right). \tag{13}$$

By performing correlation between this reference optical signal, I_{ref} with the Sagnac interferometer output signal, I_{sig}, the lock-in amplifier effectively extracts the beat-frequency component while suppressing out-of-band noise and rejecting the DC component. Signal conditioning is performed by the lock-in amplifier, featuring an internal differential preamplifier with a gain of 30. This stage reduces common-mode noise, including fluctuations in laser intensity, noise source from photodetector, and electromagnetic interference, thereby enhancing measurement stability. Theoretical simulations of noise suppression in interferometric fiber-optic gyroscopes indicate that, under a 10 kHz modulation signal and with a 1 kHz low-pass filter in the lock-in amplifier, this configuration can achieve an SNR improvement by a factor of 10 [24].

The primary goal of the gyroscope is to detect extremely low rotational speeds, i.e., when the Sagnac phase shift φ_{sag} approaches zero. To enhance the detection sensitivity of interferometric fiber optic gyroscopes at low rotation rates, this goal can be achieved by the EOM, placing in the Sagnac interferometer by employing a square wave as the driving signal for this modulator effectively induces a bias phase of $\varphi_m = \pm\pi/2$. Consequently, the detected signal can be expressed as [22]:

$$\begin{aligned} I_{\text{sig}} &= \frac{1}{8}\cos^2\theta\left[1 + \cos\left(\varphi_{\text{sag}} + \varphi_m\right)\right]\left(1 + \sin\,\omega t\right) \\ &= \frac{1}{8}\cos^2\theta\left[1 + \cos\left(\varphi_{\text{sag}} \pm \frac{\pi}{2}\right)\right]\left(1 + \sin\,\omega t\right) \\ &= \frac{1}{8}\cos^2\theta\left[1 \mp \sin\left(\varphi_{\text{sag}}\right)\right]\left(1 + \sin\,\omega t\right) \end{aligned} \tag{14}$$

Figure 3 depicts the response of the normalized optical intensity to the Sagnac phase under an applied phase bias. This bias configures the interferometer at the quadrature point, maximizing the sensitivity of the intensity output to small phase changes near zero and thus allowing for the precise measurement of low rotation rates.

4 Discussion on system scalability

The scalability of the proposed HIFOG setup, which refers to its adaptability for different measurement ranges and performance grades, is a crucial consideration for practical deployment. As governed by the Sagnac effect, the scale factor,

$$k = 2\pi LD/\lambda c \tag{15}$$

is a deterministic function of the fiber coil's physical parameters, length, L, diameter, D, and the wavelength of the light source, λ. This inherent scalability is well-supported by the key design choices in our system. Firstly, the use of a high-power, dual -frequency laser source provides a high SNR, which is essential to compensate for the increased propagation loss when longer fiber lengths are employed to achieve higher sensitivity. Secondly, the low attenuation of standard SMF makes it a cost-effective and practical medium for implementing extended coil lengths.

The simple and flexible interferometric architecture allows the system to be tailored for specific applications by adjusting L and D. For example, to achieve tactical-grade performance with moderate bias stability (e.g., 0.1–10 °/h) [25], a compact coil with shorter fiber length (e.g., 100–500 m) can be used, prioritizing small size and fast response time. Conversely, for inertial-grade applications requiring higher sensitivity and lower bias stability (e.g., <0.01 °/h) [25], the system can be scaled up using a longer fiber (e.g., 1–2 km) wound into a larger diameter coil. In such cases, the excellent coherence and power stability of the laser source become even more critical for maintaining measurement fidelity.

It is important to note that while the scale factor scales linearly with LD, other performance metrics, particularly bias stability, are also influenced by environmental factors like the Shupe effect [26], which becomes more pronounced in larger coils. Therefore, achieving optimal performance

at a scaled configuration would necessitate advanced coil-winding techniques (e.g., quadrupolar winding) [27] and precise thermal management, which are beyond the scope of this proof-of-concept study but constitute a vital direction for future investigation. The primary contribution of this work is to establish a robust and scalable core architecture. The results presented here confirm the viability of this architecture as a foundation, which can be subsequently optimized for specific performance targets through parameter scaling as discussed.

5 Conclusion and future work

In this study, we propose a method using a specially designed dual-frequency laser source that simultaneously generates two orthogonal, linearly polarized beams with a slight frequency difference. This laser source can be implemented directly using a Zeeman He–Ne laser or by combining a standard laser source with an EOM. Moreover, the frequency stability is an important issue that affect the detection performance of the proposed optical setup, a commercial frequency-stabilized Zeeman He–Ne laser can be a better choice to be a dual-frequency laser light source.

By placing a pair of parallel polarizers at both ends of the Sagnac loop, the polarization effects caused by fiber birefringence can be completely eliminated, ensuring the reciprocity of the detected light intensity signal. As a result, it is unnecessary to use polarization-maintaining fibers or polarization controllers to mitigate the birefringence effects, while still achieving maximum interference visibility.

The introduction of the dual-frequency laser source enables the generation of a time-domain interference signal through the beating phenomenon, ensuring the reciprocity of the interference signal.

In this study, we present a theoretical framework with the intention of guiding future experimental implementation. In subsequent work, we plan to transition the free-space optical setup illustrated in Figure 2 into an all-fiber configuration to construct a practical interferometric system. The actual performance of the fiber-optic gyroscope will then be systematically evaluated, with emphasis on critical metrics such as bias stability, long-term reliability study, involving continuous operation over weeks or months, temperature robustness, and laser light source stability.

The primary objective of this paper is to address the mitigation of non-ideal characteristics specific to SMF, particularly focusing on static birefringence effects. Therefore, all other optical components have been assumed ideal in the current analysis. In future experimental phases, we will expand the investigation to include the non-ideal behavior of other components, as well as dynamic birefringence effects arising from polarization mode dispersion (PMD), based on empirical measurements.

Funding information: This research was funded by the National Science and Technology Council of Taiwan under grant number NSTC 114-2221-E-182-008.

Author contribution: All authors have accepted responsibility for the entire content of this manuscript and approved its submission.

Conflict of interest: The authors state no conflict of interest.

Data availability statement: All data generated or analysed during this study are included in this published article.

References

1. Eminoglu B, Kline MH, Izyumin I, Yeh YC, Boser BE. Background calibrated MEMS gyroscope. Sensors 2014:922—5.
2. Cao H, Cai Q, Zhang Y, Shen C, Shi Y, Liu J. Design, fabrication, and experiment of a decoupled multi-frame vibration MEMS gyroscope. IEEE Sens J 2021;21:19815—24.
3. Ciminelli C, Dagostino D, Carnicella G, DellOlio F, Conteduca D, Ambrosius HPMM, et al. A high-*Q* InP resonant angular velocity sensor for a monolithically integrated optical gyroscope. IEEE Photon J 2016;8:1—19.
4. Ciminelli C, Campanella CE, Armenise MN. Optimized design of integrated optical angular velocity sensors based on a passive ring resonator. J Lightwave Technol 2009;27:2658—66.
5. Faucheux M, Fayoux D, Roland J. The ring laser gyro. J Opt 1988;19:101—15.
6. Arditty HJ, Lefevre HC. Sagnac effect in fiber gyroscopes. Opt Lett 1981;6:401—3.
7. Szafraniec B, Sanders GA. Theory of polarization evolution in interferometric fiber-optic depolarized gyros. J Lightwave Technol 1999;17:579—90.
8. Pavlath GA, Shaw HJ. Birefringence and polarization effects in fiber gyroscopes. Appl Opt 1982;21:1752—7.
9. Burns WK, Kersey AD. Fiber-optic gyroscopes with depolarized light. J Lightwave Technol 1992;10:992—9.
10. Pérez RJ, Álvarez I, Enguita JM. Theoretical design of a depolarized interferometric fiber-optic gyroscope (IFOG) on SMF-28 single-mode standard optical fiber based on closed-loop sinusoidal phase modulation with serrodyne feedback phase modulation using simulation tools for tactical and industrial grade applications. Sensors 2016;16:604.
11. Lloyd SW, Digonnet MJF, Fan S. Tactical-grade interferometric fiber optic gyroscope driven with a narrow-linewidth laser. Adv Photonics 2011:SMC3. https://doi.org/10.1364/sensors.2011.smc3.
12. Lloyd SW, Digonnet MJF, Shanhui F. Modeling coherent backscattering errors in fiber optic gyroscopes for sources of arbitrary line width. J Lightwave Technol 2013;31:2070—8.
13. Miya T, Terunuma Y, Hosaka T, Miyashita T. Ultimate low-loss single-mode fibre at 1.55 μm. Electron Lett 1979;15: 106—8.

14. Poletti F, Petrovich M, van Brakel A, Richardson D. Hollow core photonic bandgap fibre for truly single mode operation. In: 2008 IEEE/LEOS winter topical meeting series. IEEE; 2008:182—3 pp.
15. Zheng J. Birefringent fibre frequency-modulated continuous-wave Sagnac gyroscope. Electron Lett 2004;40:1520—2.
16. Zheng J. All-birefringent-fiber frequency-modulated continuous-wave Sagnac gyroscope. Opt Eng 2005;44:080501—2.
17. Zheng J. Differential all-birefringent-fiber frequency-modulated continuous-wave Sagnac gyroscope. Opt Eng 2006;45: 050501—2.
18. Su D-C, Chiu M-H, Chen C-D. Simple two-frequency laser. Precis Eng-J Int Soc Precis Eng Nanotechnol 1996;18:161—3.
19. Taksaki H. Stabilized transverse Zeeman laser as a new light source for optical measurement. Appl Opt 1980;19:3.
20. Shamir J, Fainman Y. Rotating linearly polarized light source. Appl Opt 1982;21:364—5.
21. Yu CJ, Lin CE, Yu LP, Chou C. Paired circularly polarized heterodyne ellipsometer. Appl Opt 2009;48:758—64.
22. Martin J, Winkler J. Fiber optic laser gyro signal detection and processing technique. In: Guided wave optical systems and devices I. SPIE; 1978:98—103 pp.
23. Kishore K, Akbar S. Evolution of lock-in amplifier as portable sensor interface platform: a review. IEEE Sens J 2020;20:10345—54.
24. Zhang X, Li T, Song X, Jiang C. Research on fiber-optic gyroscope signal detection with lock-in amplifier. In: 5th international symposium on advanced optical manufacturing and testing technologies: optical test and measurement technology and equipment. SPIE; 2010:426—31 pp.
25. Nayak J. Fiber-optic gyroscopes: from design to production [Invited]. Appl Opt 2011;50:E152—61.
26. Cao Y, Zhu L, Shi F, Chen Y, Cao X, Wang W, et al. Dual-polarization interferometric fiber optic gyroscope with shupe effect compensation. Appl Phys Lett 2023;123:011104.
27. Wang Z, Wang G, Wang Y, Wang Z, Gao W. Research on the birefringence distribution of the fiber coil with quadrupole symmetrical winding method. IEEE Sens J 2021;22:3219—27.